Electronic Supplementary Information

Abnormal spatial heterogeneity governing charge-carrier mechanism in efficient Ruddlesden-Popper perovskite solar cells

Jun Xi,*[ac,‡] Junseop Byeon,[ab,‡] Unsoo Kim, [ab,‡] Kijoon Bang,[ab,‡] Gi Rim Han,[d] Ji-Young Kim,[e] Jungjin Yoon,[f] Hua Dong,[g] Zhaoxin Wu,[g] Giorgio Divitini,[h] Kai Xi,[h] Jinwoo Park,[i] Tae-Woo Lee,[ij] Seong Keun Kim,[d] Mansoo Choi[ab] and Jong Woo Lee*[k]

This file includes:

Part 1. Fitting results

Part 2. Tables S1-S5

Part 3. Fig. S1-S22

References

Part 1. Fitting results in main text

1. The radiative recombination rate (k_{rad}) and nonradiative recombination rates (k_{nonrad})

The PL quantum yield (PLQY) is defined as the ratio of the radiative recombination rate (k_{rad}) and the total recombination rate (k_{tot})[1],

$$PLQY = k_{rad} / k_{tot} = k_{rad} / (k_{rad} + k_{nonrad}), \quad (1)$$

where k_{nonrad} is the nonradiative recombination rate. All PLQY results are summarized in Table S3, while k_{tot} values were identified by the exponential fitting of transient PL spectra (TRPL) (Fig. S13).

2. The diffusion lengths (L) and mobilities (μ) of charge carriers

We analyzed L and μ using the 1D diffusion models and Einstein equations[2],.

$$L \approx 2d / \pi * (2 (\tau / \tau_{quench} - 1))^{1/2}, \quad (2)$$

$$\mu = L^2 q / (kT\tau) \quad (3)$$

where d is the film thickness, τ is the carrier lifetimes of perovskites, τ_{quench} is the quenched carrier lifetimes of perovskites in transporting layers, q is the elementary charge, k is Boltzmann constant, and T is temperature. All d values are shown in Fig. S15. Additionally, τ and τ_{quench} were estimated from the time-resolved photoluminescence (TRPL) of perovskite layers (Fig. S13), and perovskite layers on transporting layers (Fig. S16). The estimated d can be found in Fig. S15.

Part 2. Supplementary tables

Table S1 Different elemental ratios of typical 3D-like (large n, here n = ∞) and 2D-like (small n, here n = 3) phases.

Element	Ratio (%) in 2D	Ratio (%) in 3D
Cs	0.145	0.255
C	9.675	1.645
I	50.6	54.0
Pb	28.2	33.3

Table S2 Statistical distribution of photovoltaic parameters for RPP solar cells using CsFMRP and MRP, respectively.

N	RPP	V_{oc} (V)	J_{sc} (mA cm^{-2})	FF (%)	PCE (%)
2	MRP	0.83±0.12	2.83±0.15	46.83±4.81	1.08±0.11
	CsFMRP	1.01±0.03	5.38±0.73	38.19±1.46	2.09±0.41
3	MRP	0.71±0.05	4.72±0.25	57.43±6.19	1.93±0.36
	CsFMRP	1.17±0.01	14.33±0.26	61.69±1.61	10.32±0.45
4	MRP	1.00±0.03	8.45±0.85	51.42±2.43	4.36±0.46
	CsFMRP	1.16±0.01	18.32±0.25	73.37±0.80	15.60±0.33

Table S3 PLQY of CsFMRP and MRP films, respectively.

PLQY (%)	CsFMRP	MRP
n = 2	0.706	0.17
n = 3	10.17	3.76
n = 4	23.6	8.37

Table S4 Dynamics of different ground state bleach (GSB) peaks of ultrafast transient absorption (TAS) spectra (Fig. 5c) for MRP and CsFMRP.

MRP		
GSB peak	First rise (ps^{-1})	Second decay (ps^{-1})
610 nm (n = 3)	/	0.039
645 nm (n = 4)	2.457	0.014
675 nm (n = 5)	2.231	0.022

CsFMRP		
GSB peak	First rise (ps^{-1})	Second decay (ps^{-1})
620 nm (n = 3)	/	0.031
750 nm (3D-like)	1.243	0.007

Table S5 Composition details of precursor solutions for MRP and CsFMRP, respectively.

MRP			
n	PbI_2 (mM)	MAI (mM)	PEAI (mM)
2	0.85	0.425	0.85
3	0.85	0.567	0.567
4	0.85	0.6375	0.425

CsFMRP						
n	PbI_2 (mM)	$PbBr_2$ (mM)	FAI (mM)	MABr (mM)	PEAI (mM)	CsI (μL/1 mL)[1]
2	0.836	0.051	0.374	0.051	0.85	28.34
3	0.832	0.068	0.4987	0.068	0.567	37.76
4	0.83	0.0765	0.561	0.0765	0.425	42.5

[1] Volume of CsI stock solutions for 1 mL CsFMRP precursor solutions. The concentration of CsI stock solutions (in DMSO) is 1.5M.

Part 3. Supplementary figures

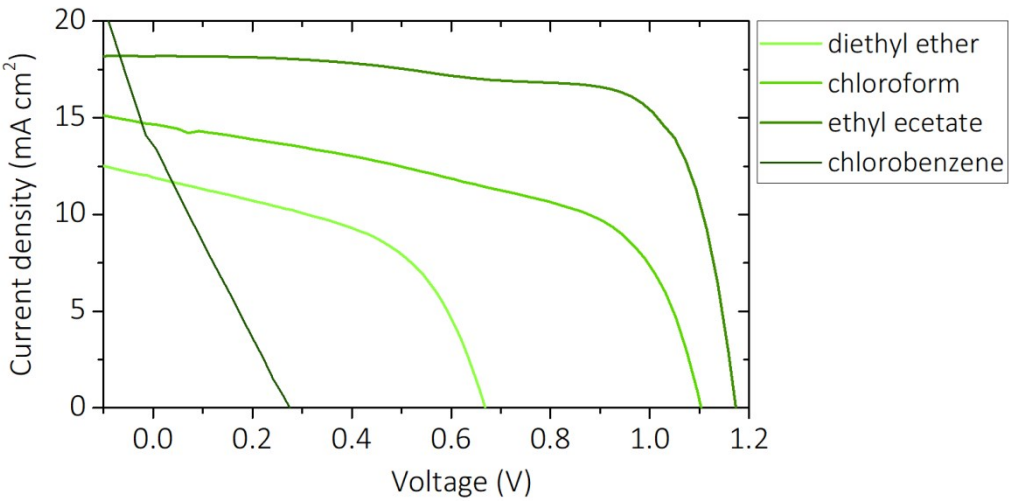

Fig. S1 J-V curves of typical CsFMRP (n = 4) perovskite solar cells driven by selective antisolvent. Traditional antisolvent chlorobenzene (CB) fails to work due to the bottom thin PTAA layer can partially dissolved by CB.

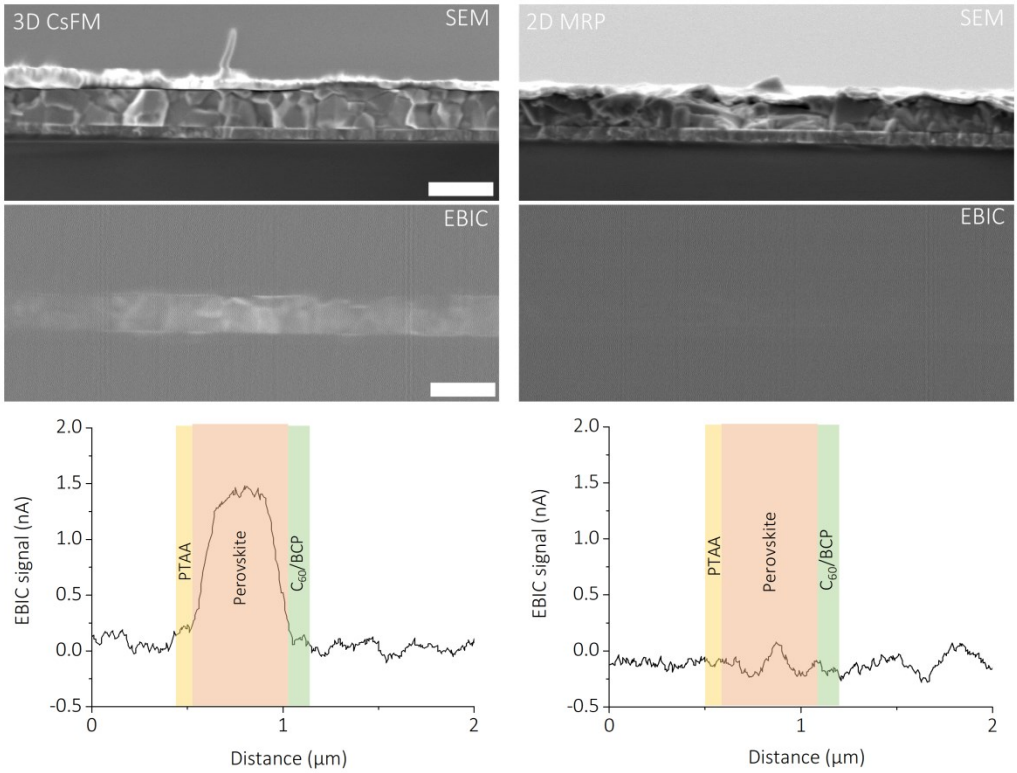

Fig. S2 Cross sectional SEM and real-time EBIC real time images of 3D triple-cation perovskites (3D CsFM) and 2D MRP (n = 4) based solar cells (scale bar: 1 μm). The bottom images show the depth profile of EBIC signals in corresponding devices.

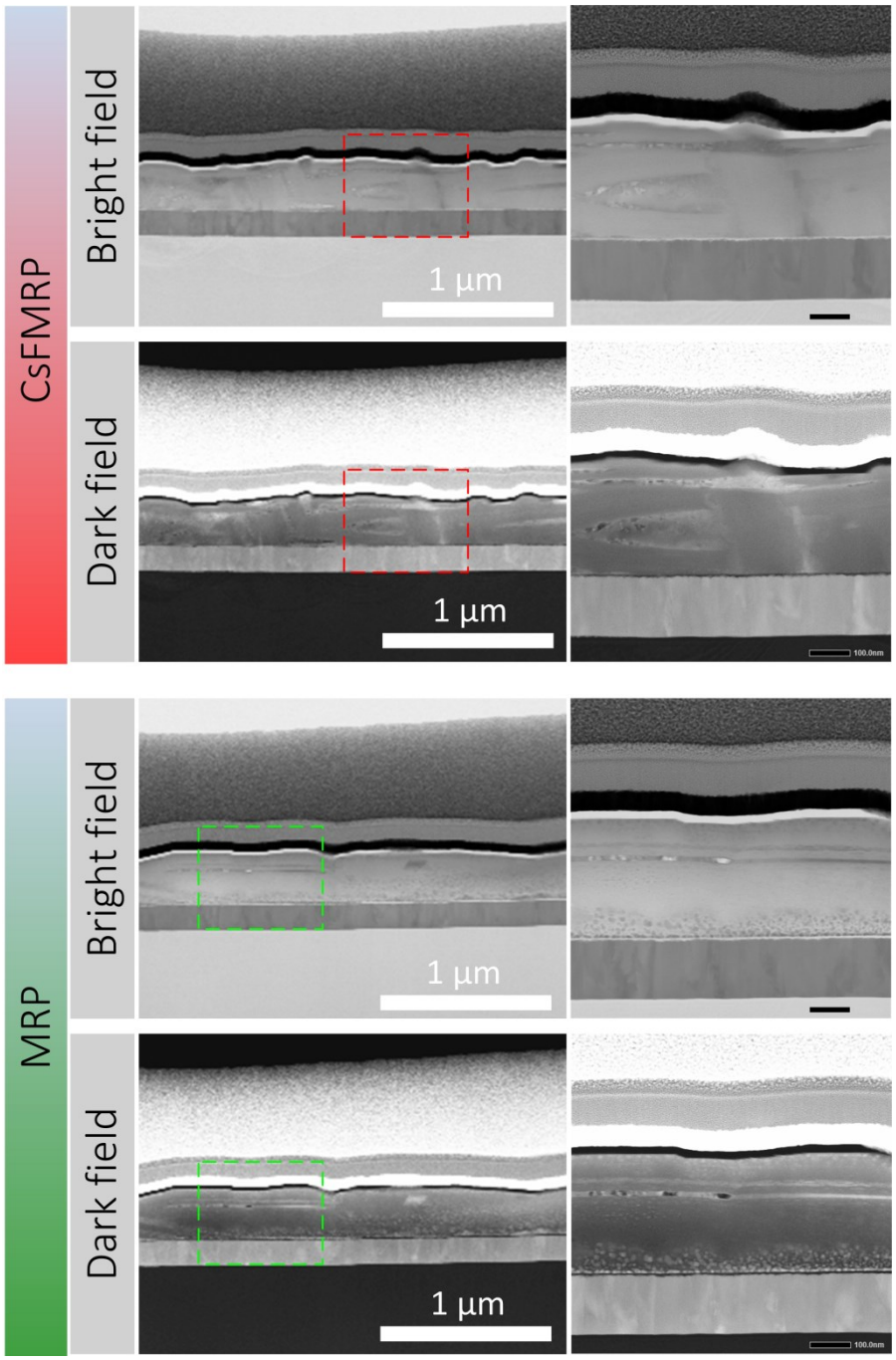

Fig. S3 Cross sectional TEM images of CsFMRP and MRP based solar cells ((n = 4), scale bar: 100 nm).

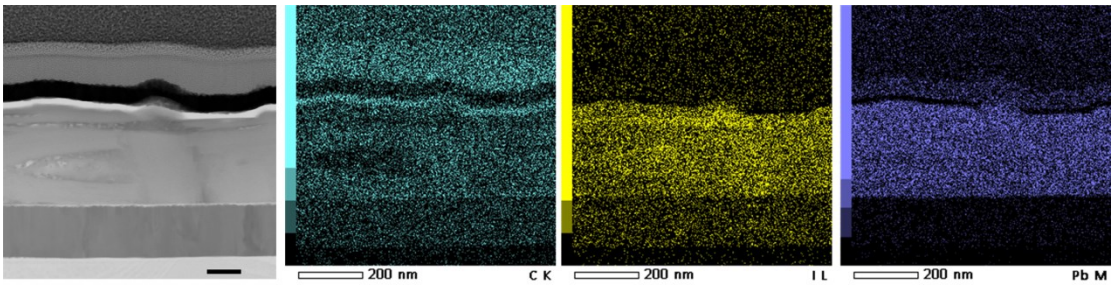

Fig. S4 Low magnified TEM image and corresponding EDS elemental maps of CsFMRP (n = 4).

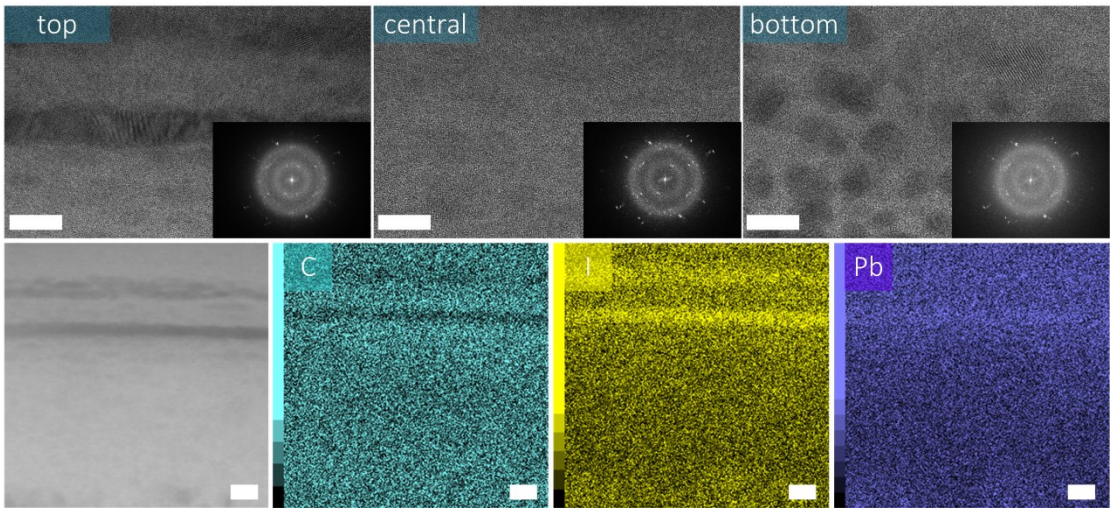

Fig. S5 High-magnification FIB-HRTEM cross sectional images and corresponding EDS elemental mappings of MRP (n = 4) perovskites based solar cells (scale bar: 20 nm).

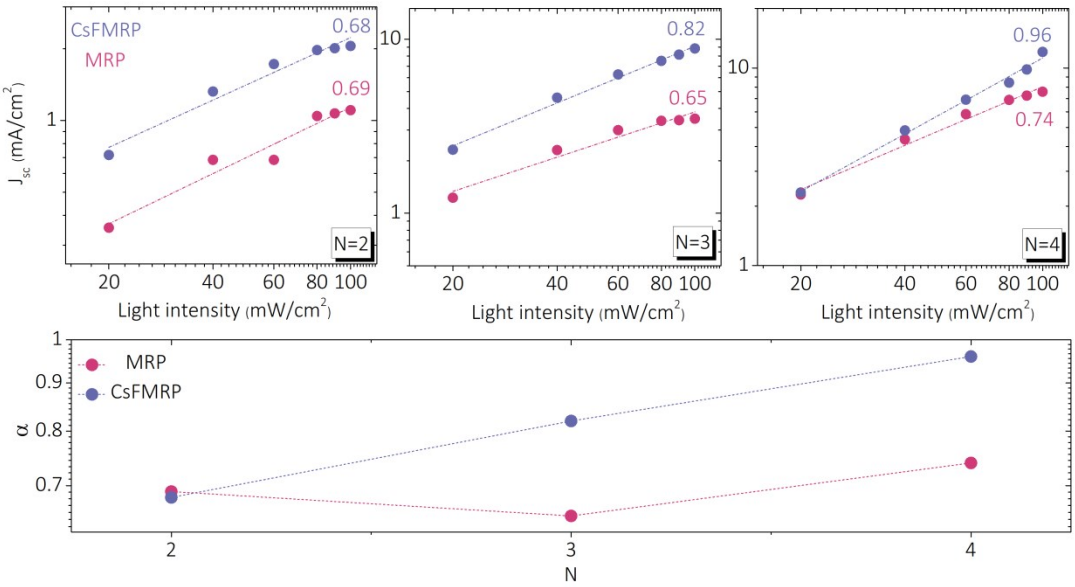

Fig. S6 Power law dependence factor α estimated as the slope of linear fitting of J_{sc} *versus* I_{int} (light-intensity).

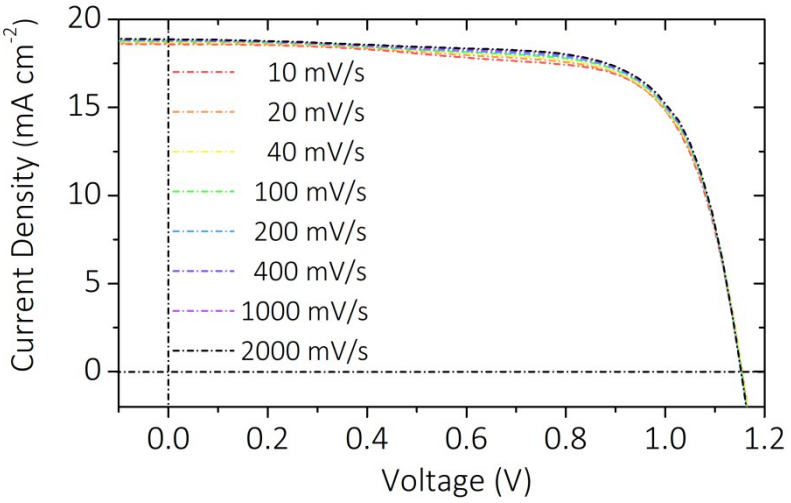

Fig. S7 J-V curves depending on different scan rates of the champion CsFMRP (n = 4) solar cells.

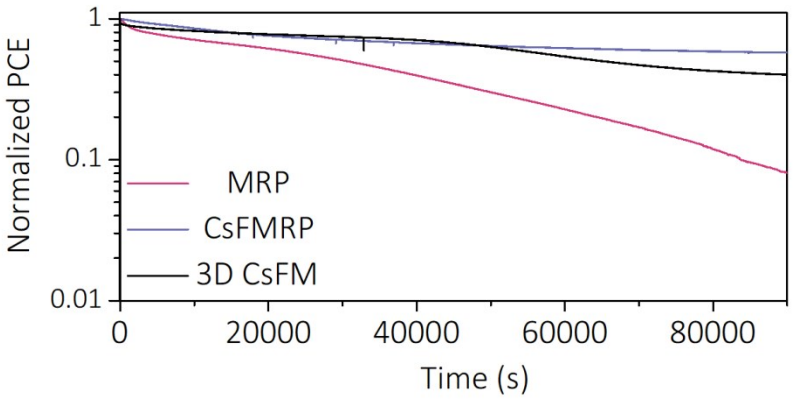

Fig. S8 Light soaking stabilities of the best devices using 2D CsFMRP, MRP (n = 4) and 3D CsFM, respectively.

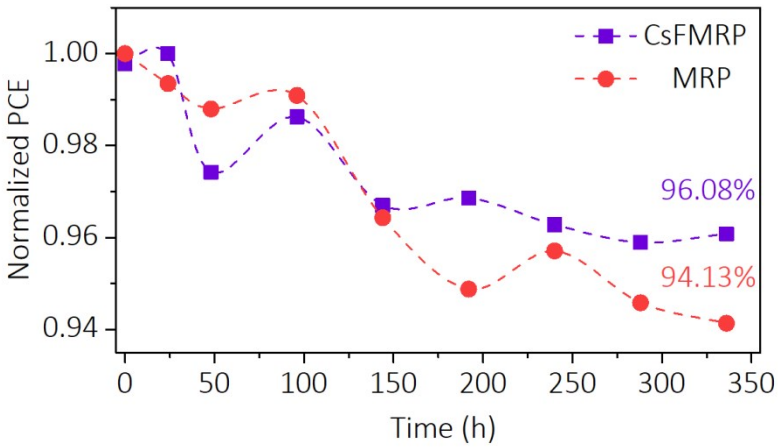

Fig. S9 Moisture stability of the non-encapsulated devices using CsFMRP and MRP stored in ambient air (~50% humidity).

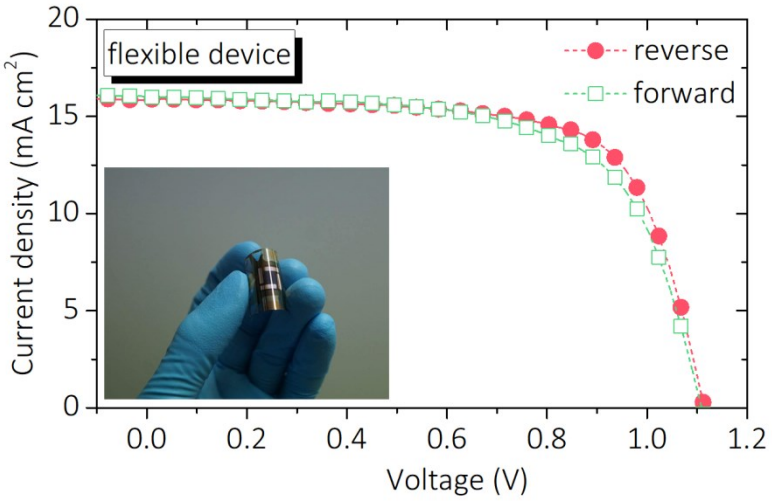

scan	V_{oc} (V)	J_{sc} (mA/cm^2)	FF (%)	PCE (%)
reverse	1.11	14.8	69.7	11.5
forward	1.11	15.0	65.0	10.8

Fig. S10 Champion flexible 2D CsFMRP (n = 4) solar cell. Little hysteresis can be found between reverse and forward scan.

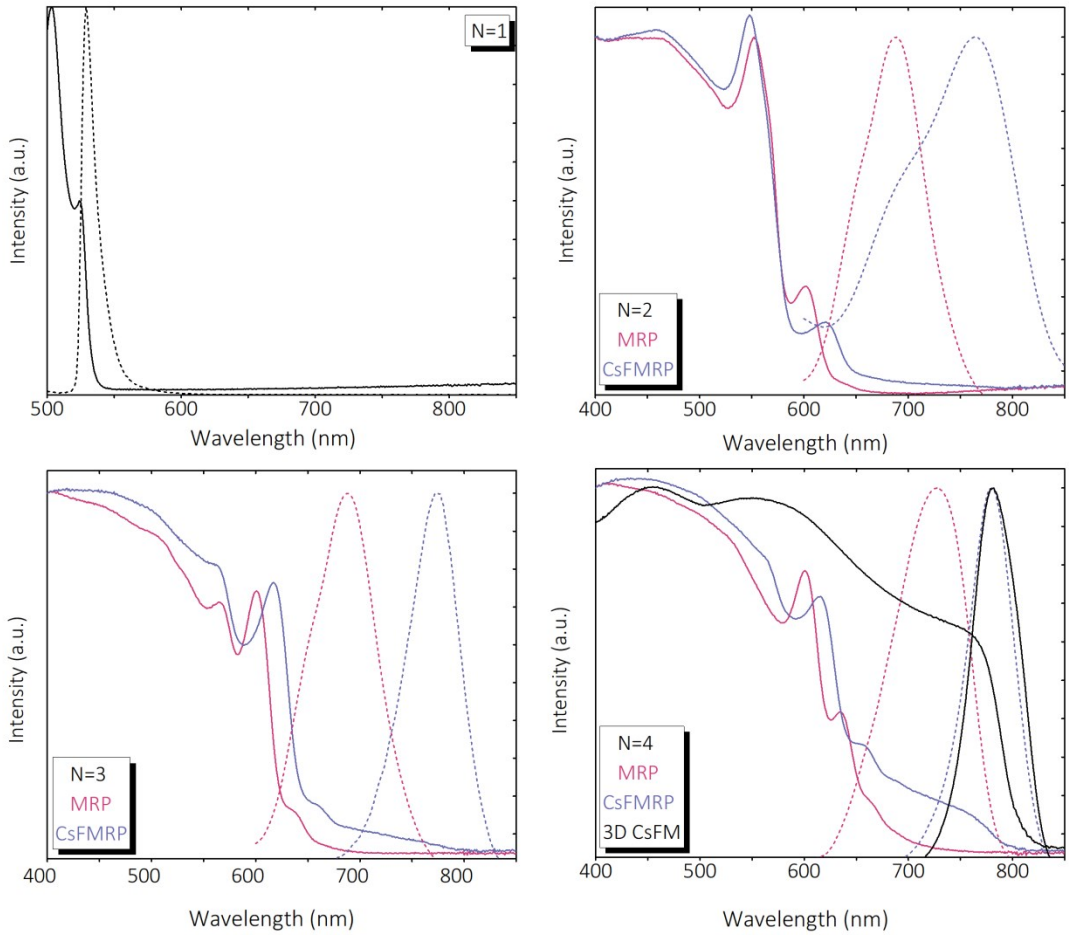

Fig. S11 UV-Vis absorption and steady-state PL spectra of different RPP films.

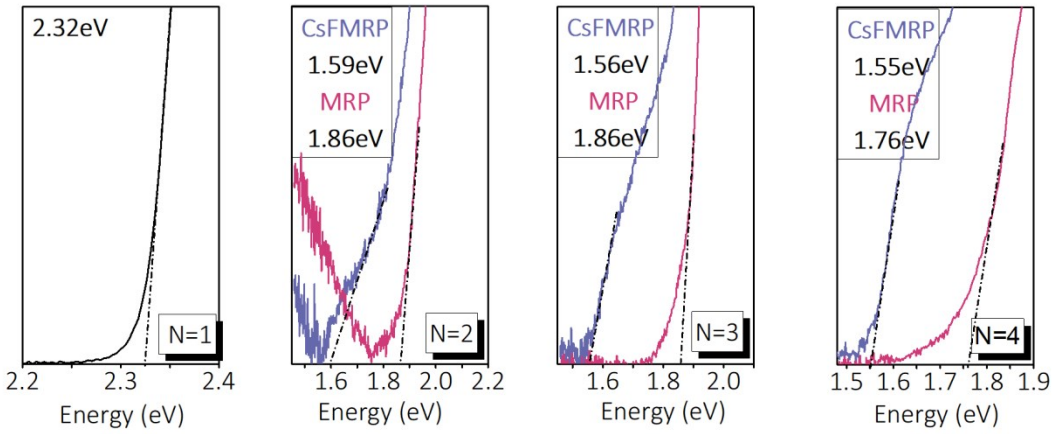

Fig. S12 Bandgap (E_g) fitting from UV-Vis absorption spectra.

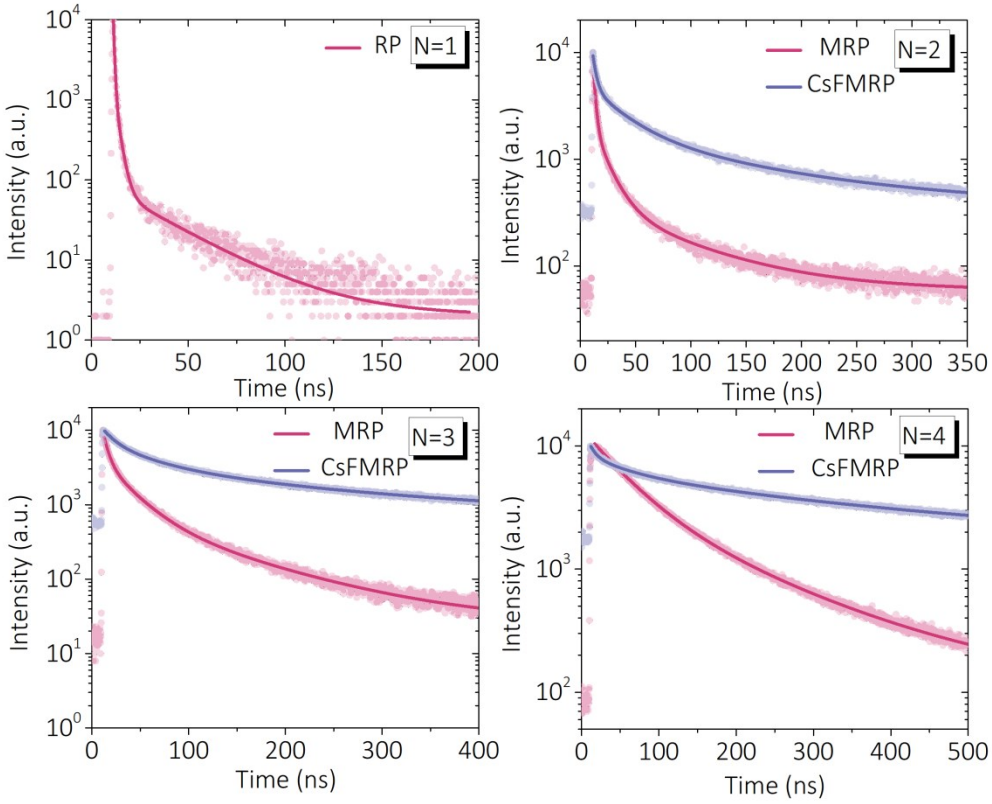

Fig. S13 Transient PL (TRPL) spectra of different RPP films on quartz. Carrier lifetime (τ) by exponential fitting of corresponding film is summarized as follows,

τ (ns)	CsFMRP	MRP
n = 1	1.06	
n = 2	38.60	10.29
n = 3	98.63	50.38
n = 4	229.40	101.04

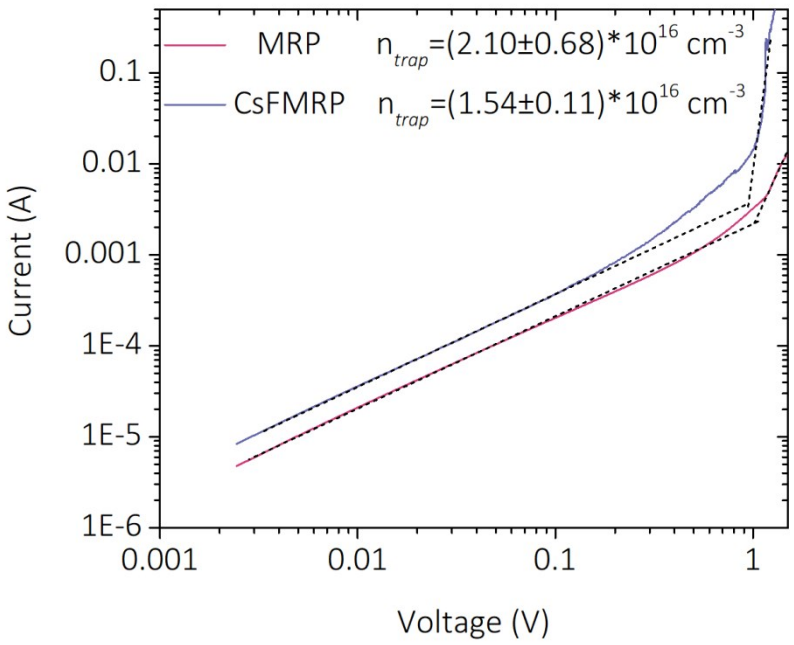

Fig. S14 Space charge limited charge (SCLC) methods to evaluate the densities of trap states.

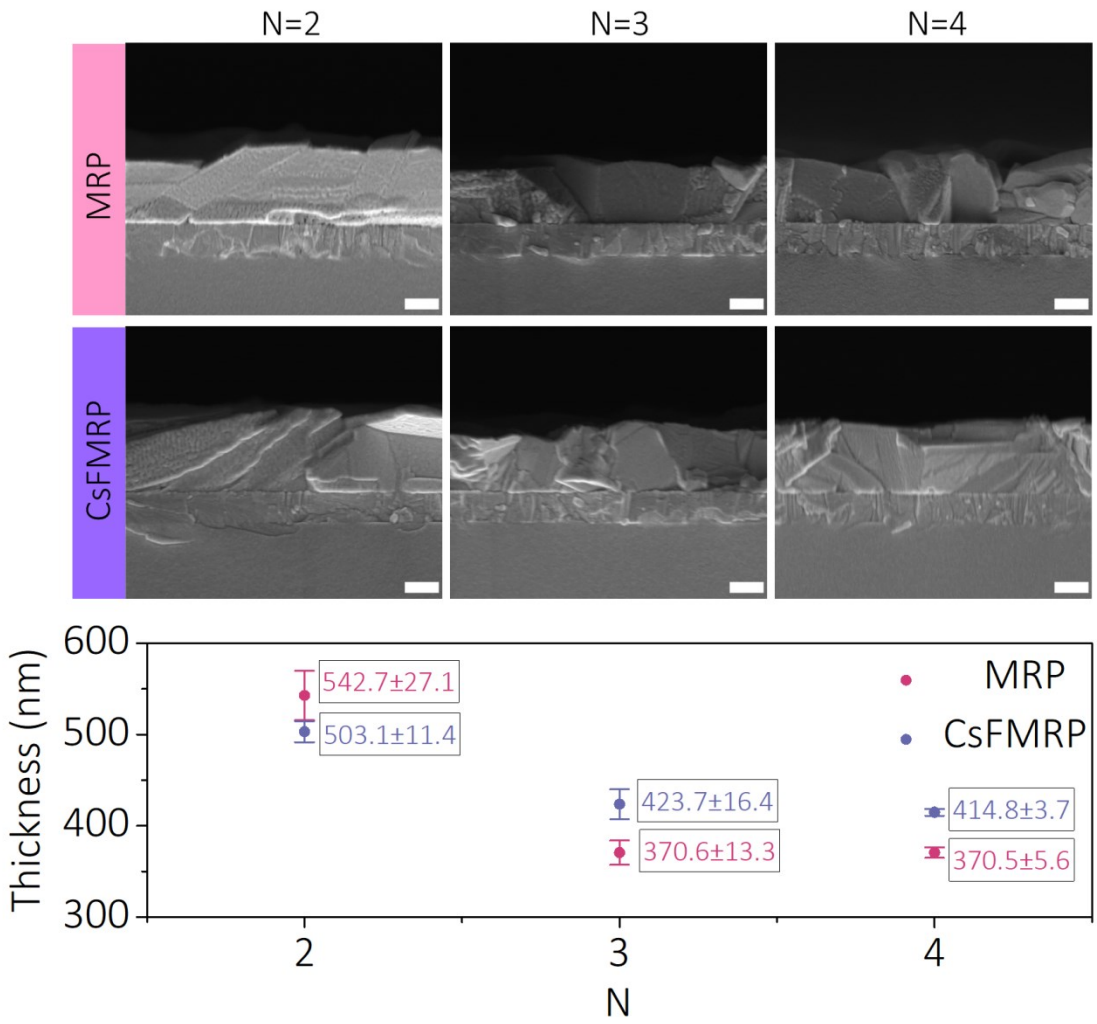

Fig. S15 Film thicknesses of different RPP films (scale bar: 200 nm).

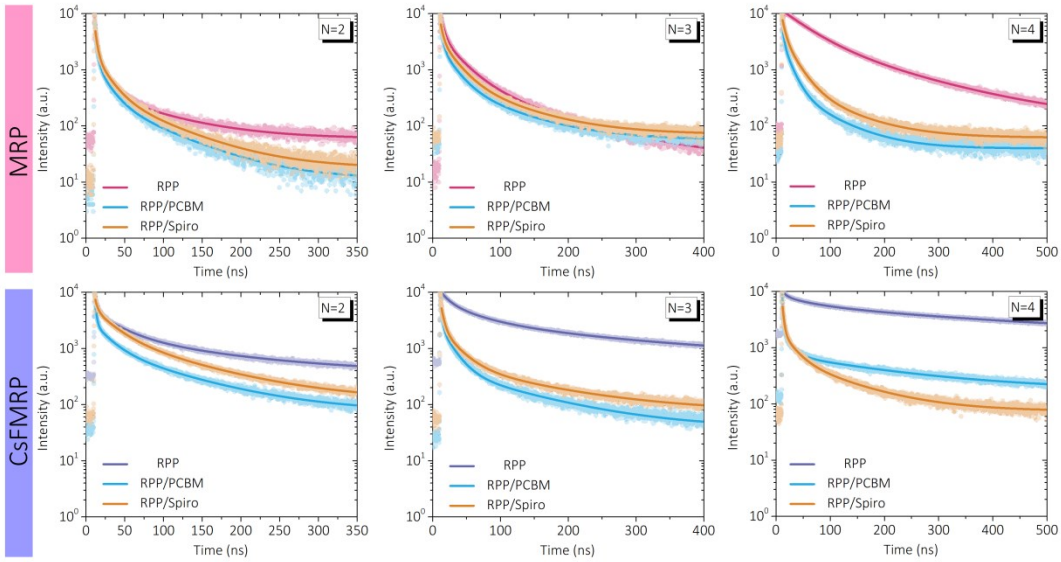

Fig. S16 TRPL spectra of different perovskites themselves and perovskites on electrons (PCBM) /holes (Spiro-MeOTAD) transporting layers. Quenched carrier lifetime (τ_{quench}) by exponential fitting of corresponding film on PCBM/Spiro-MeOTAD is summarized as follows,

τ_{quench} on PCBM (ns)	CsFMRP	MRP
n = 1	1.03	
n = 2	22.12	9.23
n = 3	10.70	15.81
n = 4	16.52	13.86

τ_{quench} on Spiro (ns)	CsFMRP	MRP
n = 1	1.01	
n = 2	30.8	9.56
n = 3	15.3	18.89
n = 4	19.13	19.16

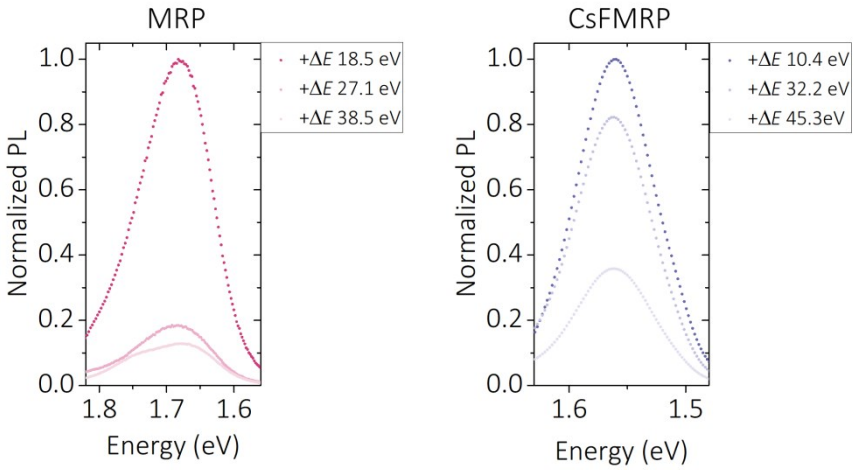

Fig. S17 Steady state PL spectra of different RPP (n = 4) using excess excitation energy beyond electronic band edges.

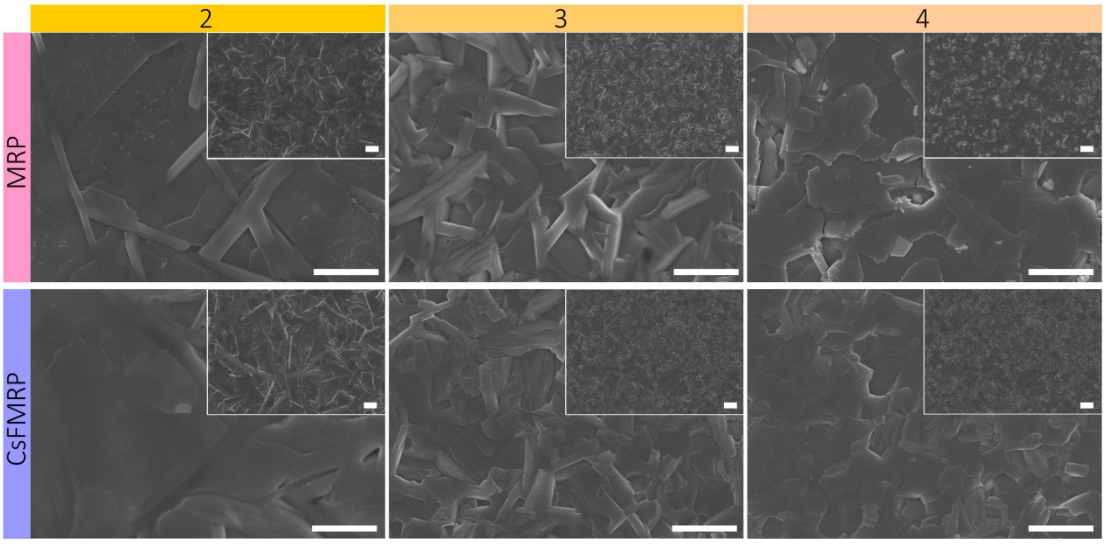

Fig. S18 Top-view SEM images of corresponding RPP films (scale bar: 1 μm in high magnification, 2 μm in low magnification).

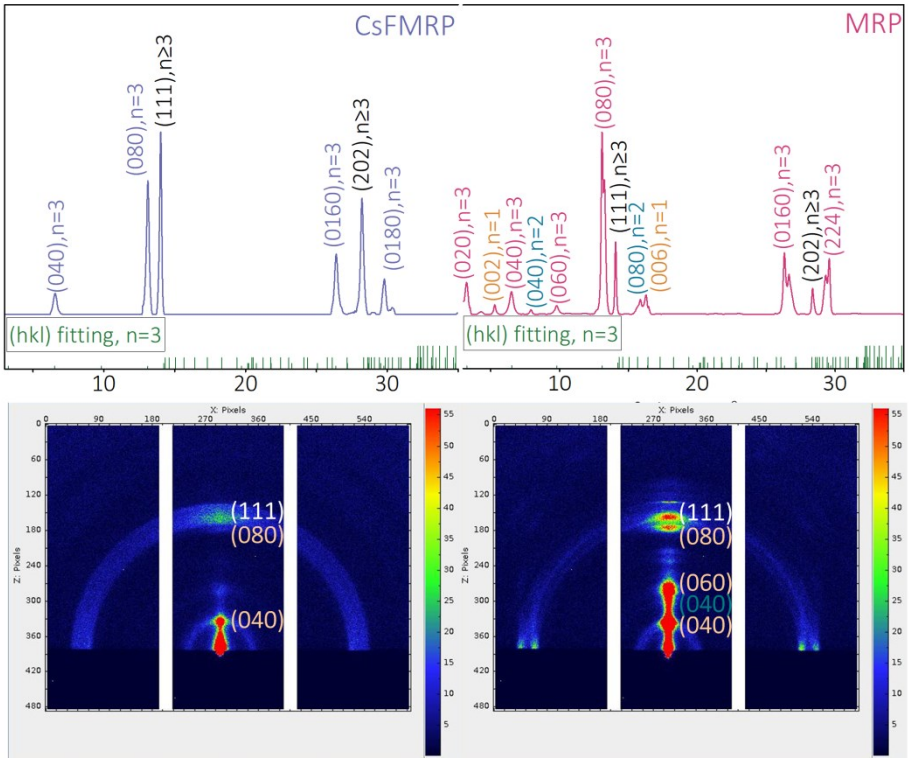

Fig. S19 XRD and related grazing-incidence wide-angle X-ray scattering (GIWAXS) images of corresponding RPP (n = 4) films. In CsFMRP, crystal phase is totally composed of ordered n = 3 phase and 3D-like (large-n) phase. In contrast, in MRP, crystal phase seems more complicated, composed of n = 1, 2, 3 phases and 3D-like (large-n) phase.

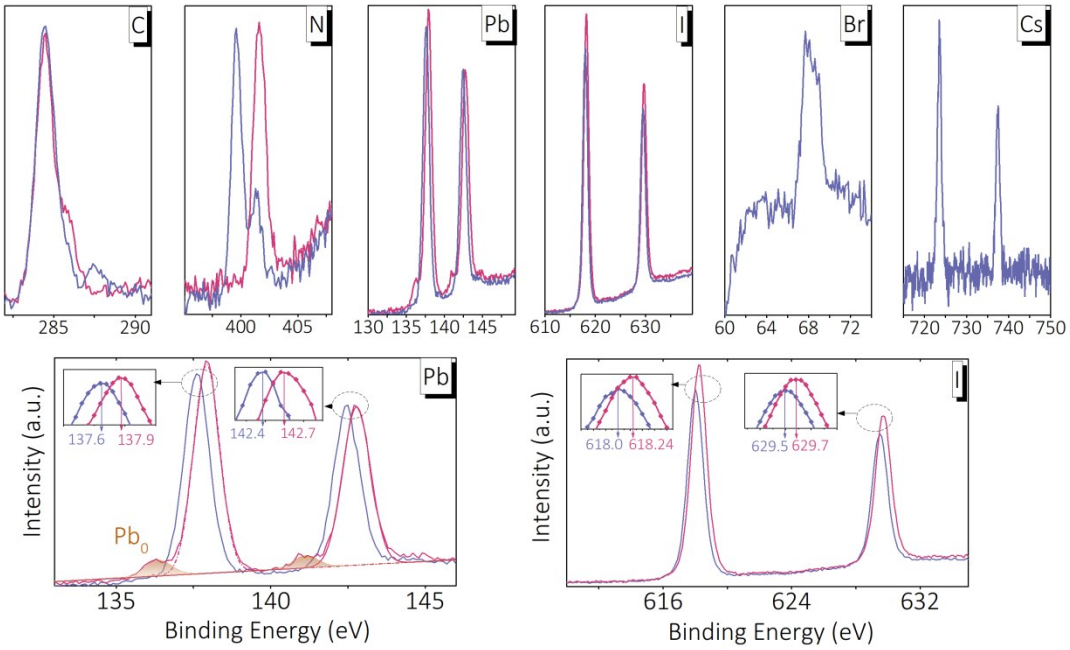

Fig. S20 XPS spectra of corresponding RPP films (n = 4), and detailed PbI_3^- cage interaction (red is MRP, blue is CsFMRP).

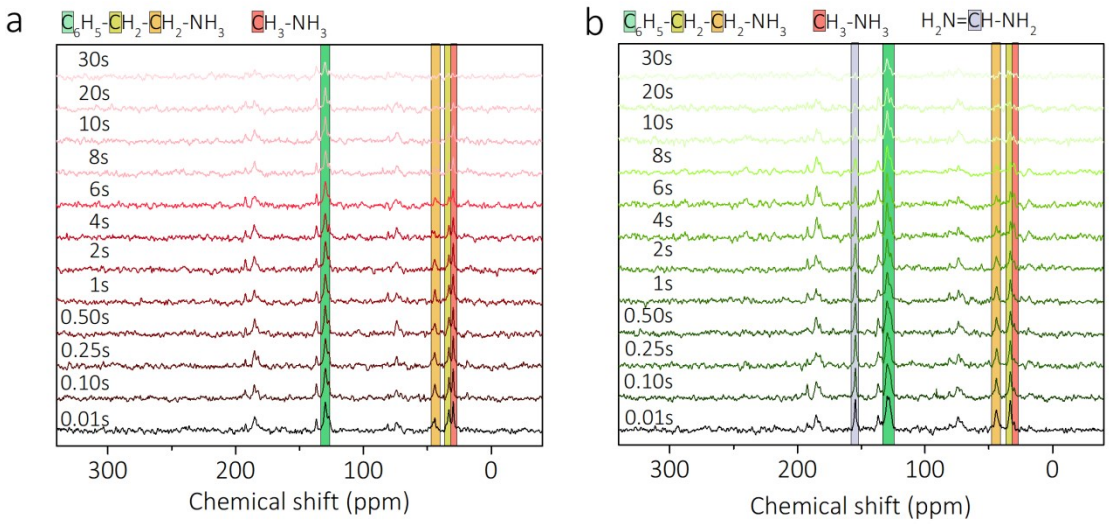

Fig. S21 Details of ^{13}C resonances in SSNMR dependent on relaxation time for (a) MRP and (b) CsFMRP.

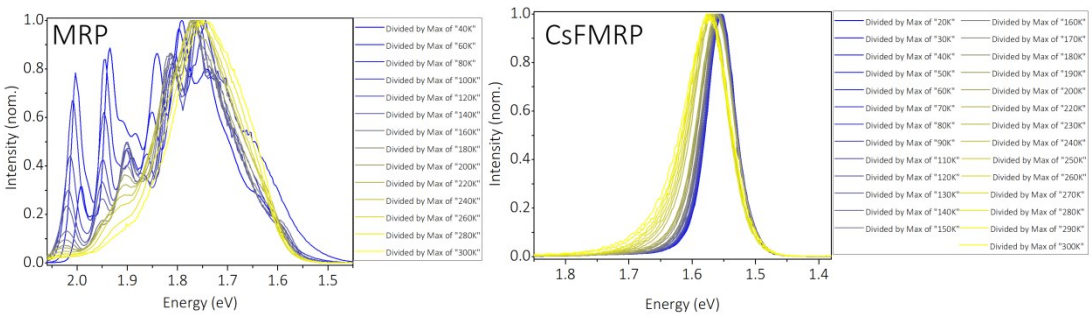

Fig. S22 Detailed normalized TPL spectra of corresponding RPP (n = 4) films.

References

1. Gong, X. et al. (2018). Electron-phonon interaction in efficient perovskite blue emitters. Nat. Mater. *17,* 550–556.
2. Proppe, A. H. et al. (2018). Synthetic control over quantum well width distribution and carrier migration in low-dimensional perovskite photovoltaics. J. Am. Chem. Soc. *140,* 2890–2896.